Nanomechanical measurements of the sequence-dependent folding landscapes of single nucleic acid hairpins

Michael T. Woodside*[†§], William M. Behnke-Parks[†], Kevan Larizadeh[†], Kevin Travers[¶], Daniel Herschlag[¶], and Steven M. Block[†‖]

*National Institute for Nanotechnology, National Research Council of Canada, Edmonton, AB, Canada T6G 2V4; and Departments of [†]Biological Sciences, [¶]Biochemistry, and [‖]Applied Physics, Stanford University, Stanford, CA 94305

Edited by Kiyoshi Mizuuchi, National Institutes of Health, Bethesda, MD, and approved February 27, 2006 (received for review December 21, 2005)

Nucleic acid hairpins provide a powerful model system for probing the formation of secondary structure. We report a systematic study of the kinetics and thermodynamics of the folding transition for individual DNA hairpins of varying stem length, loop length, and stem GC content. Folding was induced mechanically in a high-resolution optical trap using a unique force clamp arrangement with fast response times. We measured 20 different hairpin sequences with quasi-random stem sequences that were 6–30 bp long, polythymidine loops that were 3–30 nt long, and stem GC content that ranged from 0% to 100%. For all hairpins studied, folding and unfolding were characterized by a single transition. From the force dependence of these rates, we determined the position and height of the energy barrier, finding that the transition state for duplex formation involves the formation of 1–2 bp next to the loop. By measuring unfolding energies spanning one order of magnitude, transition rates covering six orders of magnitude, and hairpin opening distances with subnanometer precision, our results define the essential features of the energy landscape for folding. We find quantitative agreement over the entire range of measurements with a hybrid landscape model that combines thermodynamic nearest-neighbor free energies and nanomechanical DNA stretching energies.

DNA hairpin | energy landscape | force clamp | optical tweezers | single molecule

Hairpins formed from self-complementary sequences supply a model system for studying folding and duplex formation, the most fundamental processes for generating structure in nucleic acids. Using hairpins, repeated measurements can be made on the same molecule, facilitating single-molecule studies. Furthermore, by simply altering the nucleotide sequence, physical properties such as folding energies, kinetic rates, and distances to transition states all can be changed systematically. Hairpins also play essential roles *in vivo*. DNA hairpins bind proteins to regulate transcription (1), and hairpin intermediates are involved in both replication and recombination (2, 3). RNA hairpins form tertiary contacts (4), bind to proteins (2), regulate transcription (5), and mediate RNA interference (6). Understanding the factors that influence hairpin folding should therefore not only elucidate principles of structure formation in nucleic acids but may also shed light on the biological roles played by these structures.

Extensive calorimetric and melting studies have been carried out to generate predictive rules for the thermodynamic stability of arbitrary nucleic acid duplexes (7). The kinetic properties of duplex formation, however, remain less well understood, particularly those related to the nature of the transition state. Temperature-jump studies of annealing in short duplexes have been interpreted in terms of the nucleation of a transition state consisting of ≈1–3 bp, followed by zippering of the remaining stem (8). This interpretation, however, rests on the assumption that the enthalpy of activation arises solely from the formation of contiguous base pairs in the transition state, for which there is a lack of direct evidence. Studies of thermally induced folding in short hairpins (8–19) investigated the effects of loop structure mediated through intraloop and loop–stem interactions but have not provided any more direct means of probing the transition state. Furthermore, all of these kinetic measurements involved short, unstable duplexes because of limits on the stability of molecules that could be explored without resorting to extreme conditions.

Single-molecule studies of folding induced by mechanical means offer an alternative approach with distinct and complementary advantages. The application of force constrains a potentially complex admixture of folding pathways to a single process characterized by a dominant reaction coordinate: the molecular extension. Nanomechanical experiments follow individual folding trajectories by measuring the end-to-end extension of single molecules with extraordinary precision (20). Furthermore, this extension can be directly related to the number of base pairs formed, simplifying the interpretation of data. Especially useful is the fact that the location of the transition state along the reaction coordinate can be derived directly from the force dependence of the kinetic rates (21). The application of force also facilitates the study of molecules with a wide range of energetic stabilities under similar environmental conditions, as demonstrated by the force-induced unfolding of short duplexes (22) and hairpins (20) and very long duplexes (23–25). Nanomechanical measurements have been used to follow folding transitions in single and multiple hairpins of DNA (26) and RNA (27–30), but no attempt has yet been made to investigate systematically the effects of sequence on the folding process.

We report here optical trapping measurements comparing the folding of a variety of hairpin constructs under identical buffer and temperature conditions. Single DNA hairpins were unzipped and refolded at constant force by using an ultrastable, high-precision ($\approx$0.1 nm/$\sqrt{\text{Hz}}$ resolution) optical force clamp capable of recording transitions with rates ranging from ≈0.001 to 2,000 s^{-1} (20). The two ends of each hairpin were attached to dsDNA "handles" bound to polystyrene beads held in two independently controlled laser traps (Fig. 1*A*). By monitoring the extension of the molecule as the hairpin folded and unfolded under constant force, we measured the opening distance, the unfolding force and free energy, the force-dependent transition rates, and the location of the transition state. We investigated how each of these quantities varied for 20 different hairpin structures with quasi-random stem sequences as we altered the stem length, the loop length, and the GC content of the stem.

Conflict of interest statement: No conflicts declared.

This paper was submitted directly (Track II) to the PNAS office.

Abbreviations: FEC, force–extension curve; WLC, worm-like chain.

[§]To whom correspondence should be sent. E-mail: michael.woodside@nrc-cnrc.gc.ca.

www.pnas.org/cgi/doi/10.1073/pnas.0511048103

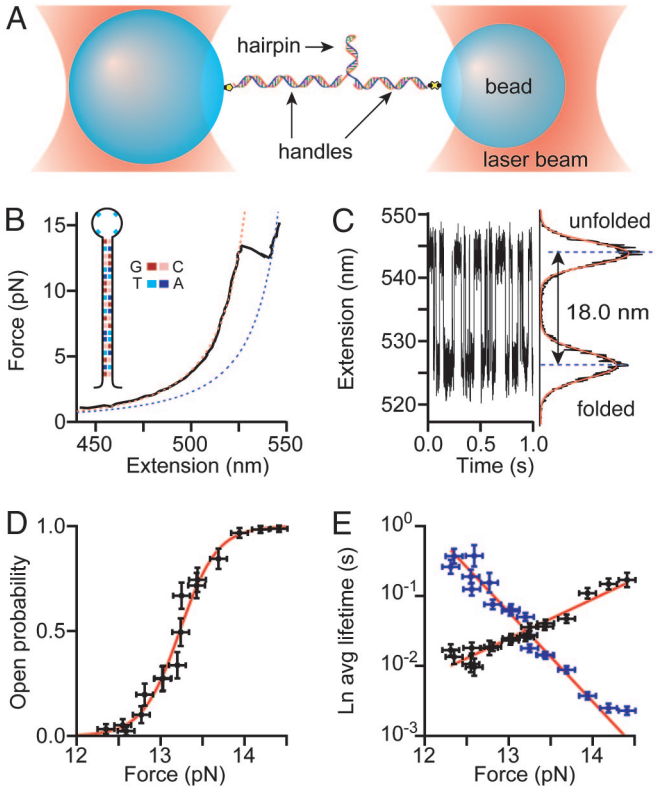

Fig. 1. Measurement of hairpin folding/unfolding. (*A*) Illustration of the experimental geometry: A hairpin is attached by means of dsDNA handles to beads held in two traps (not to scale). (*B*) FEC for hairpin 20R55/4T, displaying WLC behavior of handles at low *F* (dotted red line) followed by hairpin unfolding at ≈13 pN. WLC fit to the contour length increase after hairpin unfolding (dotted blue line) gives 17.5 ± 1 nm. (*C*) DNA extension vs. time at constant *F* reveals two-state behavior. Fit of extension histogram (black) to two Gaussian curves (red) gives an opening distance of 18.0 ± 0.5 nm. (*D*) Unfolded state probability (black) varies with *F* according to two-state Boltzmann relation (red). (*E*) Lifetimes of folded (blue) and unfolded (black) states vary exponentially with force.

Our results were then compared quantitatively with the predictions of a simple model of the folding energy landscape combining the nearest-neighbor free energies of duplex DNA with the elastic energy of unzipped DNA and the mechanical work performed by the optical trap.

Results and Discussion

Experimental Procedure. For each hairpin construct, we measured a force–extension curve (FEC), recording the force on the beads as they were separated at 10–15 nm/s. Fig. 1*B* shows a typical FEC for a hairpin consisting of a 20-bp stem with quasi-random (unpatterned) sequence, 55% GC content, and a thymidine tetraloop (denoted as hairpin 20R55/T4, where 20 indicates the stem length in base pairs, R represents the random sequence, 55 is the percentile stem GC content, and T4 indicates the loop sequence). At low forces, the FEC is well fit by a worm-like chain (WLC) model, as expected for a dsDNA molecule (31, 32). At $F \approx 13$ pN, this hairpin unfolds abruptly, producing a characteristic sawtooth pattern as the extension increases and the force drops (27). We fit the additional contour length released during unfolding to derive the opening distance, $\Delta x = 17.5 \pm 1$ nm. This distance supplies a rough estimate of 0.44 ± 0.02 nm per nt, taking into account the 2.0-nm width of duplex DNA, in good agreement with previous results (33).

Repeated folding transitions were measured at constant force by using the passive force clamp to observe from dozens to hundreds of individual transitions. The hairpin remained in thermal equilibrium throughout these measurements. A representative segment of a record for hairpin 20R55/T4 under a 13.2-pN load displays the two-state behavior noted previously (19, 20, 27), with the hairpin switching rapidly between folded and unfolded states (Fig. 1*C*). At this force, the hairpin spent roughly equal time in each state: a histogram of the extension displays two peaks well fit by Gaussian curves separated by $\Delta x = 18.0 \pm 0.5$ nm, in agreement with the opening distance obtained from the FEC. To measure directly the folded and unfolded lifetimes, we partitioned each trace into two states, using a threshold set at the midpoint between the histogram peaks. Lifetimes were exponentially distributed, as expected for a two-state system (see Fig. 4, which is published as supporting information on the PNAS web site).

The presence of two mechanical states implies that the energy landscape of the hairpin is dominated by two potential wells separated by a single barrier. The application of force tilts the energy landscape (see Fig. 5, which is published as supporting information on the PNAS web site), changing the free-energy difference between folded and unfolded states (21). By measuring the force dependence of the populations of the two states, we determined both the unfolding force, $F_{1/2}$ (defined as the force at which the hairpin has a 50% probability of being unfolded), and the free energy released, ΔG. The probability of the unfolded state as a function of force (Fig. 1*D*) fits well to the Boltzmann relation $P_u(F) = \{1 + \exp[(F_{1/2} - F)\cdot\Delta x]\}^{-1}$ (27). We found $F_{1/2} = 13.2 \pm 0.7$ pN and $\Delta x = 18 \pm 2$ nm, in good agreement with the value for Δx obtained above. The product of the unfolding force and distance gave $\Delta G = 143 \pm 12$ kJ/mol. As discussed in ref. 21, ΔG equals the hairpin unfolding free energy at zero force plus the free energy for stretching the unfolded ssDNA from $F = 0$ to $F = F_{1/2}$.

The lifetimes of the folded and unfolded states also depend on the applied force, because force changes the height of the energy barrier (Fig. 5). Assuming that the position of this barrier is force-independent, the lifetime of the folded state, τ_f, is given by $\tau_f(F) = \tau_{f,0}\cdot\exp(F\Delta x_f^{\ddagger}/k_BT)$, where $\Delta x_f^{\ddagger}$ is the distance from the folded to the transition state and $\tau_{f,0}$ is the lifetime of the folded state at $F = 0$ (21). An analogous expression holds for the lifetime of the unfolded state. From the slopes of the logarithmic average lifetimes of the folded and unfolded states as functions of force (Fig. 1*E*), we found that the transition barrier was located 12 ± 2 nm from the folded state and 5.3 ± 0.6 nm from the unfolded state. From the intercept of the fit to folded-state lifetime, we derived the unfolding rate at $F = 0$ for this hairpin, $k_{u,0} = 10^{-15\pm2}\ s^{-1}$, which, along with the unfolding free energy, supplies a measure of hairpin stability.

Energy Landscape Model. For each hairpin construct, we made a quantitative model of the folding landscape, adapting elements from previous models for dsDNA stretching (33) and unzipping (34) and RNA unfolding (27, 21, 35, 36). This model incorporates five distinct components: the energetic contributions arising from (*i*) base stacking and hydrogen bonding within the folded helix, (*ii*) stretching of the ssDNA liberated by the hairpin unfolding, and (*iii*) molecular motions in the optical trap; and the effects of elastic compliance associated with (*iv*) the ssDNA of the unfolded state and (*v*) the dsDNA handles attached to the hairpin.

The free energy required to break the base pairs in the hairpin stem sequentially was estimated from nearest-neighbor energy parameters (37) for our experimental conditions (200 mM monovalent salt and 23°C) by using MFOLD 3.1 (38). This calculation produced an energy landscape for $F = 0$ (Fig. 2*A*), to which we added the free energy for stretching the ssDNA generated as stem base pairs broke under load, estimated by using a WLC

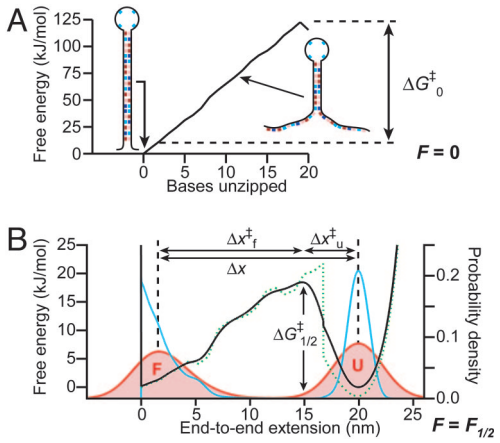

Fig. 2. Hairpin energy landscape model. (*A*) Computed free energy for sequential unzipping of base pairs in the stem for hairpin 20R55/T4 at $F = 0$ based on MFOLD. (*B*) Energy landscape at $F_{1/2}$ before (dotted green line) and after (solid black line) smoothing due to ssDNA elasticity. Barrier is close to the unfolded state; its height ($\Delta G^{\ddagger}_{1/2}$) is dominated by loop length. Hairpin extension probability density (blue line) is further smoothed by dsDNA handle elasticity to create bead position probability density (red line).

approximation (27, 32). A repulsive Morse potential (39) was added to model fluctuation-driven compression of the stem helix (i.e., negative extension), and the energy associated with stretching the fully unfolded state was included, using a WLC approximation. We then subtracted the mechanical work performed by the trap on the hairpin during unfolding, calculating the extension of the partially unzipped hairpin from previous FEC measurements of ssDNA (33) but taking into account the finite width of the stem helix as measured from NMR structures (40). Finally, we incorporated the effect of thermal fluctuations in the extension of the partially unzipped hairpin by smoothing the energy landscape by an amount proportional to the ssDNA stiffness, estimated by a WLC approximation. This model uses several simplifying assumptions: for example, we treat ssDNA as a noninteracting polymer, we neglect its enthalpic elasticity, and we assume that the applied force does not affect base-pair stacking free energies. Despite such simplifications, the model provides a practical, quantitative estimate of the folding energy landscape. See *Supporting Text*, which is published as supporting information on the PNAS web site, for more details.

An energy landscape computed for hairpin 20R55/4T is illustrated in Fig. 2*B*. The two deep wells correspond to the folded and unfolded states. Because of the unpatterned stem sequence, the steady rise in energy between these two states displays only relatively weak, sequence-specific fluctuations, followed by a steep fall upon unzipping of the last base pair and consequent release of the loop. The abrupt drop in energy near the unfolded state, attributable primarily to the release of entropy stored in the folded loop, is spread out over ≈2 nm because of the effect of ssDNA elasticity. Well depths associated with sequence-dependent fluctuations in the energy landscape are too small to trap the hairpin in intermediate minima, resulting in two-state behavior.

The behavior of hairpins was predicted quantitatively from this landscape model. First, $F_{1/2}$ was calculated as the force yielding equal probabilities for folded and unfolded states. Equal probabilities, rather than equal energy minima, is the appropriate criterion, because the potential wells associated with the two states have unequal widths (Fig. 2*B*). The compliance of the dsDNA handles attached to the hairpin elastically filters any hairpin motions transmitted to the trapped beads. This effect was incorporated by smoothing the probability density for the hairpin extension, generating a modeled extension histogram (Fig. 2*B*) similar to the experimental result (Fig. 1*C*). From the energy landscape and extension histograms, we obtained predictions for Δx, ΔG, the barrier heights at F_0 and $F_{1/2}$, and the barrier location along the reaction coordinate. For all hairpins, model predictions were averaged over the same range of WLC parameters consistent with previous measurements: ssDNA persistence length of 1.0–1.5 nm (33, 41–44) and contour length per nucleotide of 0.58–0.67 nm (45).

Comparison of Measurements and Model. We measured the folding of 20 different hairpins with a wide variety of structures and stabilities, observing the effects of systematic changes in stem length, loop length, and stem GC content. Results are graphed in Fig. 3. Numerical values are listed in Table 1, which is published as supporting information on the PNAS web site, and representative records are shown in Fig. 6, which is published as supporting information on the PNAS web site. Fig. 3 *A–F* shows results for hairpins with identical tetraloops and stems ranging in length from 6 to 30 bp, sharing the same sequence at each end of the stem (hairpins 6R50/4T, 8R50/4T, 10R50/4T, 15R53/4T, 20R50/4T, 25R52/4T, and 30R50/4T; sequences are listed in Table 2, which is published as supporting information on the PNAS web site). Fig. 3 *G–L* shows results for hairpins with identical 15-bp stems but loop sizes ranging from 3 to 30 nt (hairpins 15R60/3T, 15R60/4T, 15R60/6T, 15R60/8T, 15R60/12T, 15R60/15T, 15R60/20T, and 15R60/30T). Polythymidine loops were chosen to minimize any loop structure arising from intraloop stacking interactions (15, 46). Fig. 3 *M–R* shows results for hairpins with thymidine tetraloops and 20-bp unpatterned stem sequences as the GC content was varied from 0 to 100% (hairpins 20R0/4T, 20R25/4T, 20R50/4T, 20R55/4T, 20R75/4T, and 20R100/4T).

The opening distance measured directly from extension histograms (Fig. 3 *A*, *G*, and *M*) increased roughly linearly with stem length and loop length but varied little with GC content, as expected. The small rise with increasing GC content is caused by the increase in $F_{1/2}$ for more stable hairpins, which produces a larger extension per nucleotide (33). The measured Δx values agree well with predictions of the landscape model, confirming previous measurements of the mechanical properties of ssDNA. The only discrepancies were observed for the hairpins with the longest loops, which we attributed to measurement drift associated with the long lifetimes of these hairpins. We note that the model predicts that the nominally "folded" state actually consists of an admixture of fully folded and partially unfolded hairpins (by 1–3 bp; Fig. 2*B*). This fraying, analogous to thermal breathing of the duplex (46), is consistent with statistical mechanical calculations of RNA hairpin unfolding under load (21). It represents a general, but previously neglected, feature of mechanically induced folding that must be taken into account when interpreting such measurements. Based on our findings, failure to account for fraying results in predicted values for the opening distance that are consistently at least 1–2 nm too large.

The unfolding force rose nonlinearly with stem length, decreased with increasing loop length, and increased linearly with stem GC content, in excellent agreement with model predictions (Fig. 3 *B*, *H*, and *N*). The increase in $F_{1/2}$ with stem length and GC content follows from the increasing energetic stability of the hairpin. The decrease with increasing loop length follows from the increasing energy stored in longer loops, which reduces the work performed by the optical trap to equalize the populations of folded and unfolded states. These data cover the complete range of forces that can be expected for unfolding DNA. Previous work on phage λ DNA found that kilobase-long duplexes with ≈50% GC content unzip at an average force of ≈15 pN (23–25). Our results indicate that this asymptotic value is reached at a duplex length of only ≈25 bp. Extrapolating the

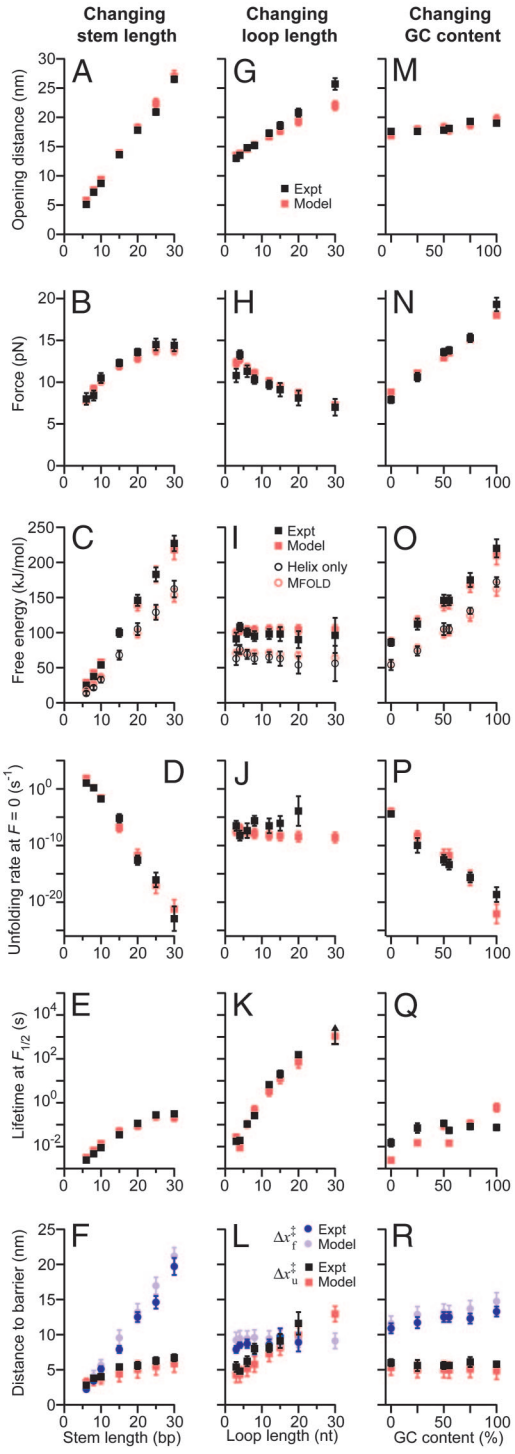

Fig. 3. Summary of results for hairpins with varied stem length (*A–F*), loop length (*G–L*), and stem GC content (*M–R*). Error bars represent sum of standard and systematic errors (experiment) or standard deviation of predictions over the full parameter set (model). (*A*, *G*, and *M*) Hairpin opening distance rises linearly with stem and loop length but is little changed with GC content (experiment, black; model, red). (*B*, *H*, and *N*) Unfolding force rises nonlinearly with stem length to a plateau at ≈25 bp, falls with loop length, and rises linearly with GC content. (*C*, *I*, and *O*) Unfolding free energy rises linearly with stem length and GC content but is little changed with loop length. Open circles show free energy of helix stacking only. (*D*, *J*, and *P*) Unfolding rate extrapolated to $F = 0$ decreases exponentially with increasing stem length and GC content but is little changed with loop length. (*E*, *K*, and *Q*) Folding lifetime at $F_{1/2}$ rises exponentially with loop length but depends much less strongly on stem length and GC content. (*F*, *L*, and *R*) Distance to transition state from folded state (experiment, blue; model, purple) rises linearly with stem length, whereas distance from unfolded state (experiment, black; model, red) rises linearly with loop length, consistent with a transition state located 1–2 bp from loop.

results of Fig. 3*N*, we expect $F_{1/2}$ for long duplexes to vary linearly with GC content from ≈9 pN (at 0% GC content) to ≈21 pN (at 100%), consistent with previous work on poly(AT) and poly(GC) duplexes (26).

The unfolding free energy, ΔG, depended only on the properties of the stem, rising linearly with both stem length and GC content (as expected) but varying little with loop length (Fig. 3 *C*, *I*, and *O*). We found excellent agreement with the free energy predicted by our model over one order of magnitude, confirming that single-molecule unfolding measurements offer a robust, accurate means of determining equilibrium free energies. Subtracting the entropic contribution to ΔG from ssDNA stretching (representing approximately a quarter of the total free energy), we obtained the duplex stacking free energies (open circles in Fig. 3*C*, *I*, and *O*). These values agree well with the predictions of MFOLD after taking into account fraying of the stem as discussed above. Our data therefore provide independent confirmation of the validity of the thermodynamic nearest-neighbor energies for DNA, showing clearly that values measured by single-molecule force spectroscopy over a wide range of sequences agree very well with those derived from bulk assays.

The unloaded unfolding rate, $k_{u,0}$, decreased exponentially with increasing stem length and GC content but was insensitive to loop length (Fig. 3 *D*, *J*, and *P*). These trends can be understood in terms of the energy landscape for $F = 0$ (Fig. 2*A*). For all hairpins we studied, the model predicts that $\Delta G^{\ddagger}_0$, the barrier height at $F = 0$, corresponds to the energy for melting all but the last base pair in the stem (minus the energy of any frayed base pairs in the folded state under load). Hence, linear increases in stem free energy arising from changes in stem length or GC content produce exponential decreases in $k_{u,0}$. To compare model and experiment, we expressed $k_{u,0}$ as $k_{u,0} = \kappa_u \cdot \exp(-\Delta G^{\ddagger}_0/k_BT)$, where the prefactor, κ_u, depends on the viscous damping because of drag on the hairpin, the handles, and the beads, as well as on the shape of the potential landscape (47). Assuming that drag on the beads and handles predominates, κ_u should be similar for all constructs. We therefore fit the data to the modeled barrier heights by using a single parameter, $\kappa_u = 3 \times 10^6\ s^{-1}$. The predictions and measurements agree remarkably well over ≈25 orders of magnitude in rate for all hairpins studied. The rates at $F = 0$ are also consistent with rates from fluorescence and temperature-jump studies of short DNA and RNA hairpins with 2- to 9-bp stems (14–19, 48, 49), from optical trapping studies of longer RNA hairpins with ≈20-bp stems (27, 28), and from temperature-jump studies of the helix-coil transition in duplexes (8). The present measurements, however, greatly expand the range of stability that has been explored and connect these diverse findings (see Fig. 7, which is published as supporting information on the PNAS web site).

The unfolding lifetime at $F_{1/2}$, $\tau_{1/2}$, varied roughly exponentially with both stem length and loop length but was ≈100 times more sensitive to loop length, rising approximately five orders of magnitude (Fig. 3 *E*, *K*, and *Q*; only a lower bound could be placed on $\tau_{1/2}$ for the most stable hairpin, 15R60/T30). In contrast, $\tau_{1/2}$ varied little with GC content. This behavior is precisely that predicted by the energy landscape model (Fig. 2*B*). For hairpins with random stem sequences, the barrier height is set mostly by the energy for unfolding or reforming the loop under load. Expressing the lifetime as $\tau_{1/2} = \tau^0_{1/2} \cdot \exp(\Delta G^{\ddagger}_{1/2}/k_BT)$, where $\Delta G^{\ddagger}_{1/2}$ is the barrier height at $F_{1/2}$, we fit the data by using a single parameter, $\tau^0_{1/2} = 1 \times 10^{-5}$ s (allowing different values for prefactors $\tau^0_{1/2}$ and κ_u because of qualitatively different

landscapes at $F_{1/2}$ and $F = 0$). The model agrees very well over six orders of magnitude in lifetime with the data for varying stem and loop lengths. It also captures the qualitative effects of changing stem GC content but predicts slightly larger changes in $\tau_{1/2}$ than were observed. This discrepancy is likely caused by simplifying assumptions in the WLC model used to calculate the loop energies to which $\Delta G^{\ddagger}_{1/2}$ is sensitive. Effects such as the enthalpic component of DNA elasticity, ignored here, would tend to reduce the predicted rise in $\Delta G^{\ddagger}_{1/2}$ with GC content.

Changing the closing base pair (i.e., the base pair nearest the loop) from AT to GC, which increased the stem GC content by 5% and only minimally raised hairpin stability as measured by ΔG or $k_{u,0}$, nevertheless had a pronounced effect on $\tau_{1/2}$, reducing it by a factor of approximately three (compare hairpins 20R50/T4 and 20R55/T4). The lifetime is reduced because the transition state is very close to the loop (see below and Fig. 2*B*); hence, stabilizing the closing base pair reduces the barrier between the unfolded and transition states. To achieve a comparable variation in $\tau_{1/2}$ by changing base pairs distributed randomly in the stem, one-quarter or more of the stem sequence had to be changed, emphasizing the dominant contribution of the loop to the height of the energy barrier. Single base-pair changes thus exert significant effects on the folding of hairpins with random stem sequences only when located adjacent to the loop.

Turning finally to the position of the energy barrier, we found that it was located roughly midway between folded and unfolded states for short hairpins but remained close to the unfolded state for long hairpins, never moving $>\approx$6 nm away (Fig. 3*F*). As the loop length increased, the barrier maintained a constant distance from the folded state (Fig. 3*L*). As the GC content was varied, the barrier distance was constant from both the folded and unfolded states (Fig. 3*R*). These observations are fully consistent with the model, which predicts a barrier located in the stem a few base pairs from the loop. Its position changes little with GC content but moves away from the unfolded state when the loop is lengthened and away from the folded state when the stem is lengthened.

Taken at face value, the measured opening distances imply that the transition state involves the formation of ≈1.5–5 bp adjacent to the loop, depending on stem length. In comparison, the "raw" energy landscapes (without elastic smoothing effects, illustrated by the dotted line in Fig. 2*B*) suggest that approximately 1–2 bp would be formed in the transition state, placing it closer to the unfolded state than actually measured. This apparent discrepancy arises from the neglect of the elastic compliance of the ssDNA generated during the unfolding. The ssDNA elasticity smoothes the otherwise abrupt drop in energy upon release of the loop, in effect pushing the energy barrier further from the unfolded state. When elasticity is taken properly into account, our experimental results imply a transition state consisting of 1–2 bp adjacent to the loop. Previous measurements of the activation enthalpies for short duplexes and hairpins were consistent with the formation of 1–3 contiguous, canonical bp, but such studies could not distinguish this simple model of the transition state from alternatives that would return identical enthalpy values through combinations of hydrogen bonding, base stacking, and solvation. Our measurements agree with the 1–3 bp previously postulated (8, 15, 22, 44, 50–52) and provide the most direct evidence thus far for the formation of contiguous base pairs in the transition state for duplex association and dissolution. We note that the absence of tertiary structure has been proposed to generate a "compliant" transition, where the transition state is located midway between folded and unfolded states (27, 53). Our results show clearly that this situation does not obtain in general. These earlier conclusions regarding the location of the transition state therefore appear to relate only to the specific sequences studied, which happened to generate barriers closer to the middle of the stem (35).

By measuring the mechanically induced folding of individual DNA hairpins with a variety of sequences at high resolution and under constant environmental conditions, we have systematically studied the sequence-dependent folding landscape for nucleic acid duplexes. The power of these techniques, the simplicity of the folding landscape under force, and the wealth of available biochemical and physical information have allowed us to describe quantitatively the folding of hairpins by a straightforward model for the energy landscape that incorporates key features of the thermodynamic and mechanical properties of DNA. Our results provide strong evidence that the transition state for duplex formation involves ≈2 consecutive base pairs. The agreement of the model with the data is especially remarkable in light of the physical details neglected, such as solvent effects and viscous drag on the hairpin (52), base stacking and other self-interactions in ssDNA, and enthalpic elasticity. Further precision measurements of hairpin folding should enable more stringent tests of the energy landscape formalism through experiments designed to probe the limits of applicability of the physical assumptions and studies of more irregular landscapes formed by hairpins containing patterned stem sequences and structured loops.

Methods

DNA Hairpin Constructs. Each construct consisted of a single short DNA hairpin attached at its 5′ and 3′ ends to long dsDNA handles used for pulling. Constructs were based on PAGE-purified DNA oligomers (Integrated DNA Technologies, Coralville, IA) containing the desired hairpin sequence (Table 2). Abasic sites (deoxyribose spacers) were incorporated in the oligomers at each end of the hairpin sequence to disrupt potential base-stacking interactions between the hairpin stem and the DNA handles. A 23-nt PCR primer was placed at the 3′ end of the oligomers, and a nonpalindromic ligation sequence was placed at the 5′ end. Autosticky PCR (54) using the primer region of the oligomer generated a 621-bp segment of dsDNA with the hairpin as a 5′ overhang at one end and a digoxigenin label at the other end, adapting a previous approach (22). The PCR product was ligated at 24°C with T4 DNA ligase (New England Biolabs) to a biotin-labeled, 1,036-bp fragment of dsDNA with a 5′ overhang complementary to the ligation sequence at the 5′ end of the hairpin oligomer. The final ligation product was gel-purified.

Hairpin constructs were incubated for 1 h at ≈22°C with 600-nm diameter polystyrene beads (Bangs Laboratories, Carmel, IN) coated with avidin-DN (Vector Laboratories) and 730-nm diameter beads coated with polyclonal anti-digoxigenin (Roche Diagnostics). Incubations were performed with all ingredients at ≈50 pM in 6 mM Tris/40 mM phosphate buffer, pH 7.5/0.05% Tween 20, producing "dumbbells" consisting of the DNA construct bound to one bead of each type at either end (55). Dumbbells were diluted 100-fold in assay buffer consisting of 50 mM Mops, pH 7.5/200 mM KCl/2% oxygen scavenger solution (250 mg/ml glucose/37 mg/ml glucose oxidase/1.7 mg/ml catalase).

Optical Trap. Measurements were performed at 23 ± 0.5°C with an optical trapping apparatus as described (20). Two traps produced by orthogonally polarized infrared laser beams were used to exert force on beads at either end of a dumbbell (Fig. 1*A*). The positions and intensities of the traps were controlled by acousto-optic deflectors. Bead displacements in each trap were measured independently with two orthogonally polarized detector beams from a HeNe laser. Light scattered by the beads was separated by polarization and collected by position-sensitive detectors (Pacific Silicon Sensor, Westlake Village, CA), whose

signals were amplified by home-built normalizing differential amplifiers, filtered, and digitized. Trap stiffness was determined by standard techniques, and bead positions in each trap were calibrated for each dumbbell measured (56). For steady-state measurements, hairpin extension was recorded for 5–4,500 s (depending on the folding rate), sampled at 0.2–20 kHz, filtered online with an eight-pole Bessel filter at 0.1–10 kHz, and filtered offline by a median filter with a 1- to 10,000-ms window.

Repeated folding transitions at constant force were measured by using a passive force clamp: one of the traps was made weaker than the other, and the bead held in it was pulled to the edge of the trap, where the local stiffness became zero, and hence the force was nearly constant for small displacements (20). In this arrangement, changes in the end-to-end extension of the hairpin construct were measured in the weak trap, without any need for elastic compliance corrections. Force was measured in the strong trap, where the bead remains stationary, based on a calibrated stiffness of 0.3–0.4 pN/nm. Force was set by modulating the light intensity in the weak trap. The passive force clamp used here aids the study of hairpin folding by removing artifactual force changes caused by finite feedback response times and by allowing the measurement of rapid transitions with lifetimes down to 0.5 ms.

Hairpins with very short unfolding distances or low unzipping forces (hairpins 6R50/4T, 8R50/4T, 10R50/4T, 15R50/4T, 15R60/3T, 15R60/4T, and 20R0/4T) were also measured in an unclamped configuration, where both beads were held in the harmonic regions of their respective traps (stiffness of each trap was 0.3–0.4 pN). This method allowed folding transitions to be better resolved by increasing the total system stiffness and hence reducing the Brownian noise. Comparisons of force-clamped and unclamped measurements on the same hairpins showed no appreciable difference in behavior (data not shown).

Dumbbells with more than one DNA molecule were detected by measuring the FEC at forces below the unzipping force and determining the persistence length, L_p, from a fit to the WLC model. Multiple tethers, characterized by low L_p values, were discarded.

We thank J. Shaevitz for help with instrument development, E. Abbondanzieri for discussions on the folding landscape, P. Anthony for help with sample preparation, and members of S.M.B.'s laboratory and the Ribozyme Folding Project for advice and support. This work was supported by National Institutes of Health Grant P01-GM066275.

1. Glucksmann-Kuis, M. A., Dai, X., Markiewicz, P. & Rothman-Denes, L. B. (1996) *Cell* **84,** 147–154.
2. Varani, G. (1995) *Annu. Rev. Biophys. Biomol. Struct.* **24,** 379–404.
3. Gellert, M. (2002) *Annu. Rev. Biochem.* **71,** 101–132.
4. Brion, P. & Westhof, E. (1997) *Annu. Rev. Biophys. Biomol. Struct.* **26,** 113–137.
5. Wang, D., Meier, T. I., Chan, C. L., Feng, G., Lee, D. L. & Landick, R. (1995) *Cell* **81,** 341–350.
6. Yu, Y. J., DeRuiter, S. L. & Turner, D. L. (2002) *Proc. Natl. Acad. Sci. USA* **99,** 6047–6052.
7. Serra, M. J. & Turner, D. H. (1995) *Methods Enzymol.* **259,** 242–261.
8. Pörschke, D. (1977)) *Mol. Biol. Biochem. Biophys.* **24,** 191–218.
9. Senior, M. M., Jones, R. A. & Breslauer, K. J. (1988) *Proc. Natl. Acad. Sci. USA* **85,** 6242–6246.
10. Antao, V. P. & Tinoco, I., Jr. (1992) *Nucleic Acids Res.* **20,** 819–824.
11. Vallone, P. M., Paner, T. M., Hilario, J., Lane, M. J., Faldasz, B. D. & Benight, A. S. (1999) *Biopolymers* **50,** 425–442.
12. Proctor, D. J., Ma, H., Kierzek, E., Kierzek, R., Gruebele, M. & Bevilacqua, P. C. (2004) *Biochemistry* **43,** 14004–14014.
13. Baxter, S. M., Greizerstein, M. B., Kushlan, D. M. & Ashley, G. W. (1993) *Biochemistry* **32,** 8702–8711.
14. Hilbers, C. W., Haasnoot, C. A., de Bruin, S. H., Joordens, J. J., van der Marel G. A. & van Boom, J. H. (1985) *Biochimie* **67,** 685–695.
15. Ansari, A., Kuznetsov, S. & Shen, Y. (2001) *Proc. Natl. Acad. Sci. USA* **98,** 7771–7776.
16. Bonnet, G., Krichevsky, O. & Libchaber, A. (1998) *Proc. Natl. Acad. Sci. USA* **95,** 8602–8606.
17. Goddard, N., Bonnet, G., Krichevsky, O. & Libchaber, A. (2000) *Phys. Rev. Lett.* **85,** 2400–2403.
18. Wallace, M. I., Ying, L., Balasubramanian, S. & Klenerman, D. (2001) *Proc. Natl. Acad. Sci. USA* **98,** 5584–5589.
19. Grunwell, J. R., Glass, J. L., Lacoste, T. D., Deniz, A. A., Chemla, D. S. & Schultz, P. G. (2001) *J. Am. Chem. Soc.* **123,** 4295–4303.
20. Greenleaf, W. J., Woodside, M. T., Abbondanzieri, E. A. & Block, S. M. (2005) *Phys. Rev. Lett.* **95,** 208102.
21. Tinoco, I., Jr., & Bustamante, C. (2002) *Biophys. Chem.* **101–102,** 513–533.
22. Lang, M. J., Fordyce, P. M., Engh, A. M., Neuman, K. C. & Block, S. M. (2004) *Nat. Methods* **1,** 133–139.
23. Essevaz-Roulet, B., Bockelmann, U. & Heslot, F. (1997) *Proc. Natl. Acad. Sci. USA* **94,** 11935–11940.
24. Bockelmann, U., Thomen, P., Essevaz-Roulet, B., Viasnoff, V. & Heslot, F. (2002) *Biophys. J.* **82,** 1537–1553.
25. Danilowicz, C., Coljee, V. W., Bouzigues, C., Lubensky, D. K., Nelson, D. R. & Prentiss, M. (2003) *Proc. Natl. Acad. Sci. USA* **100,** 1694–1699.
26. Rief, M., Clausen-Schaumann, H. & Gaub, H. E. (1999) *Nat. Struct. Biol.* **6,** 346–349.
27. Liphardt, J., Onoa, B., Smith, S. B., Tinoco, I., Jr., & Bustamante, C. (2001) *Science* **292,** 733–737.
28. Onoa, B., Dumont, S., Liphardt, J., Smith, S. B., Tinoco, I., Jr., & Bustamante, C. (2003) *Science* **299,** 1892–1895.
29. Harlepp, S., Marchal, T., Robert, J., Léger, J.-F., Xayaphoummine, A., Isambert, H. & Chatenay, D. (2003) *Eur. Phys. J. E Soft Matter* **12,** 605–615.
30. Li, P. T. X., Collin, D., Smith, S. B., Bustamante, C. & Tinoco, I., Jr. (2006) *Biophys. J.* **90,** 250–260.
31. Smith, S. B., Cui, Y. & Bustamante, C. (1996) *Science* **271,** 795–799.
32. Marko, J. F. & Siggia, E. D. (1995) *Macromolecules* **28,** 8759–8770.
33. Dessinges, M.-N., Maier, B., Zhang, Y., Peliti, M., Bensimon, D. & Croquette, V. (2002) *Phys. Rev. Lett.* **84,** 248102.
34. Lubensky, D. K. & Nelson, D. R. (2002) *Phys. Rev. E Stat. Nonlin. Soft Matter Phys.* **65,** 031917.
35. Cocco, S., Marko, J. F. & Monasson, R. (2003) *Eur. Phys. J. E Soft Matter* **10,** 153–161.
36. Manosas, M. & Ritort, F. (2005) *Biophys. J.* **88,** 3224–3242.
37. SantaLucia, J., Jr. (1998) *Proc. Natl. Acad. Sci. USA* **95,** 1460–1465.
38. Zuker, M. (2003) *Nucleic Acids Res.* **31,** 3406–3415.
39. Peyrard, M. & Bishop, A. R. (1989) *Phys. Rev. Lett.* **62,** 2755–2758.
40. van Dongen, M. J., Mooren, M. M., Willems, E. F., van der Marel, G. D., van Boom, J. H., Wijmenga, S. S. & Hilbers, C. W. (1997) *Nucleic Acids Res.* **25,** 1537–1547.
41. Tinland, B., Pluen, A., Sturm, J. & Weill, G. (1997) *Macromolecules* **30,** 5763–5765.
42. Rivetti, C., Walker, C. & Bustamante, C. (1998) *J. Mol. Biol.* **280,** 41–59.
43. Wuite, G. J. L., Smith, S. B., Yong, M., Keller, D. & Bustamante, C. (2000) *Nature* **404,** 103–106.
44. Kuznetsov, S. V., Shen, Y., Benight, A. S. & Ansari, A. (2001) *Biophys. J.* **81,** 2864–2875.
45. Murphy, M. C., Rasnick, I., Cheng, W., Lohman, T. M. & Ha, T. (2004) *Biophys. J.* **86,** 2530–2537.
46. Saenger, W. (1984) *Principles of Nucleic Acid Structure* (Springer, New York).
47. Hänggi, P., Talkner, P. & Borkovec, M. (1990) *Rev. Mod. Phys.* **62,** 251–341.
48. Menger, M., Eckstein, F. & Pörschke, D. (2000) *Biochemistry* **39,** 4500–4507.
49. Jung, J. & van Orden, A. (2005) *J. Phys. Chem. B* **109,** 3648–3657.
50. Zhang, W. & Chen, S.-J. (2002) *Proc. Natl. Acad. Sci. USA* **99,** 1931–1936.
51. Sorin, E. J., Rhee, Y. M., Nakatani, B. J. & Pande, V. S. (2003) *Biophys. J.* **85,** 790–803.
52. Ansari, A. & Kuznetsov, S. (2005) *J. Phys. Chem. B* **109,** 12982–12989.
53. Tinoco, I., Jr., Collin, D. & Li, P. T. X. (2004) *Biochem. Soc. Trans.* **32,** 757–760.
54. Gal, J., Schnell, R., Szekeres, S. & Kalman, M. (1999) *Mol. Gen. Genet.* **260,** 569–573.
55. Shaevitz, J. W., Abbondanzieri, E. A., Landick, R. & Block, S. M. (2003) *Nature* **426,** 684–687.
56. Neuman, K. C. & Block, S. M. (2004) *Rev. Sci. Instr.* **75,** 2787–2809.

Supporting Text

Hairpin Sequences. The hairpin sequences are listed in Table 2; nomenclature is described in the text. Occasionally, hairpin constructs broke before measurements were completed over a range of forces sufficient to determine the load dependence of the rates. For some other constructs (particularly for stable hairpins with very slow transition rates), measurements were only carried out near $F_{1/2}$, precluding determination of the force-dependent rates. In such cases, only a partial data set was obtained (typically, sufficient to determine the quantities Δx, ΔG, $F_{1/2}$, and/or $\tau_{1/2}$). The number of molecules, n, for which complete data sets were obtained is listed in the table; the value in parentheses indicates the total number of molecules measured.

Effect of External Force on a Two-State Energy Landscape. As described previously (1), the application of force tilts the energy landscape, changing the relative free energies of the folded, unfolded, and transition states, and hence the populations of the folded and unfolded states and the transition rates between them (Fig. 5). The location of the transition state is assumed to be independent of force, as mentioned in the text (1, 2). This approximation is valid in the limit of a sharp barrier potential: a change in force of ΔF shifts the transition state position by $\Delta F/\kappa$, where κ is the stiffness (curvature) of the potential landscape at the transition state.

Exponential Kinetics. As expected for a stochastic, two-state process, the lifetimes of the folded and unfolded states under constant load were exponentially distributed. Distributions for the lifetime of the unfolded state of hairpin 20R55/T4 at two different forces are shown in Fig. 4.

Hairpin Energy Landscape Model. The model of the energy landscape for hairpin folding includes three free-energy components (the free energy of base-pair stacking and hydrogen bonding in the stem, the free energy for stretching the ssDNA released by unzipping, and the free

energy associated with displacement under load in the optical trap) plus two stiffness components (the stiffness of ssDNA released by unzipping and the stiffness of the dsDNA handles).

Energetic Components. The free energy of base-pair stacking and hydrogen bonding was calculated from nearest-neighbor free energy parameters ("Turner rules") using MFOLD 3.1, applying corrections for the temperature (23°C) and salt content of the assay buffer (200 mM; monovalent). Because of the use of force to unfold the hairpins, base pairs in the helix are constrained to unzip and reform sequentially. As each base pair unzips, it releases not only energy stored in base-pairing interactions, but also two nucleotides of ssDNA that are stretched by the applied force. The extension per nucleotide produced at the unfolding force was calculated from the ssDNA FEC measured by Dessinges *et al*. (3) at low salt concentrations, where secondary structure formation is disfavored. The free energy for stretching the ssDNA was computed from a simple WLC interpolation formula that neglects enthalpic contributions to the ssDNA stiffness (4). Because a range of parameter values exists in the literature for the persistence length, L_p, and contour length, L_0, of ssDNA, we estimated the stretching energy using 41 different combinations of these experimental parameters, with L_p ranging from 1.0 to 1.5 nm and L_0 from 0.58 to 0.67 nm per nucleotide. Model prediction uncertainties were estimated from the variance produced in calculations based on this range of parameter values, assuming, in addition, a 5% error in the ssDNA FEC (3). The work performed by the optical trap was calculated simply as the force, F, times the hairpin extension, x. Finally, compression of the stem helix (which is driven by Brownian fluctuations and would correspond to a negative value of hairpin extension) was described by a Morse potential, $V(x) = \varepsilon[1-\exp(-x/a)]^2$, using parameter

values consistent with previous work: $\varepsilon = 2.5\ k_B T$ and $a = 0.018$ nm (5). The free-energy landscape from these energetic contributions is given by:

$$\Delta G(F,x) = \Delta G_{mfold}(x) + \Delta G_{stretch}(x) + F \cdot x \qquad , x \geq 0;$$

$$= \varepsilon\left[1 - \exp\left(-x/a\right)\right]^2 + F \cdot x \qquad , x < 0, \qquad [1]$$

where $\Delta G_{stretch}(x) = \frac{k_B T}{L_p} \frac{L_0}{4(1 - x/L_0)} \left[3(x/L_0)^2 - 2(x/L_0)^3\right]$.

The actual change in extension upon breaking the last base pair holding the stem together must take into account the geometry of the hairpin helix. We calculated this distance from NMR structures of a DNA hairpin with a 6-bp stem (6), PDB ID code 1AC7. The dsDNA handles in our assay undergo a small (~30º) bend at the locus of attachment to the hairpin stem, because of the applied force. We assumed that this curvature is taken up by the single-stranded abasic sites at the 5′ and 3′ ends of the hairpin stem. As the last base pair in the helix breaks during unfolding, the bending constraints at these points of handle attachment are relieved. This releases an additional DNA extension, associated with both the distance subtended by the bending and the structural distance between the two attachment points on the stem helix, which was incorporated into an "effective helix width" of 2.0 nm.

We note that the free energy associated with the loop was included in the model both through the entropic free energy for stretching the ssDNA in the unfolded loop and through the loop free-energy parameters in MFOLD. In all hairpins studied, the loop contained only thymidine residues in order to minimize potential intraloop structure. Intraloop enthalpic terms beyond those accounted for empirically in MFOLD, although they can be important for loops with more complex sequences (7), are therefore not expected in this work.

The simplifying assumption that the ssDNA stretching free energy is purely entropic overestimates the free energy at high external loads, where enthalpic contributions become increasingly important.

Stiffness Components. The elasticities of both the dsDNA handles and the ssDNA released upon unfolding affect the folding behavior observed in the optical trap. Because ssDNA is elastic, thermal fluctuations in the end-to-end extension of the hairpin (the reaction coordinate) under tension lead to a fluctuating number of unzipped base pairs. We approximated this effect by smoothing the "raw" energy landscape (Eq. 1) over a distance $\sigma(x) = [k_B T/k_{ss}(x)]^{1/2}$, where $k_{ss}(x)$ is the stiffness of the ssDNA estimated from the slope of the WLC model for the FEC. Optical trapping experiments do not measure hairpin extension directly, because the hairpin is connected to the beads through dsDNA handles. For the same reasons given above, the effect of elasticity in these handles is to smooth the extension probability distribution of the hairpin, $p(x) \propto \exp[-\Delta G(x)/k_B T]$. To reproduce the extension histogram measured experimentally, we modeled this effect by convolving the computed extension probability density with a Gaussian function whose width is comparable to that observed for fluctuations in a dsDNA tether of comparable length without a hairpin.

Representative Records. Fig. 6 displays excerpts from records of hairpin unfolding and refolding under constant loads, along with the corresponding extension histograms. Hairpins where the stem length was varied are shown in Fig. 6*A*, hairpins where the loop length was varied are shown in Fig. 6*B*, and hairpins where the GC content was varied are shown in Fig. 6*C*. The inset cartoons in Fig. 6 show the color-coded hairpin sequence. In all instances, the two-state transitions are evident, and Gaussian fits to the histograms, corresponding to the folded and unfolded states, are shown (Fig. 6, red lines). All records (except that of hairpin 8R50/T4) were

obtained under force-clamped conditions, as described (see *Methods*). Note that the initial extension of the hairpin in the folded state varies from molecule to molecule, despite identical contour lengths of the dsDNA handles. This is attributable to variations in the bead radii and the different forces applied to the hairpins.

Numerical Data. Table 1 displays experimental values and model fits associated with the results presented in Fig. 3. Hairpin folding data were acquired at a temperature estimated to be 23 ± 0.5°C, a value that incorporates heating by the optical trapping laser itself, which we estimated to raise the sample temperature by 2.0 ± 0.5°C (8). For each hairpin, experimental averages are given in Table 1, with model results shown in italics below. Uncertainties in experimental data were computed from the statistical standard error of the mean (calculated by bootstrap analysis) added in quadrature to an estimate of the systematic error associated with calibration uncertainties and heterogeneity in bead size. Uncertainties in the model results represent the standard deviation of the results calculated using the range of parameter values described above.

Measurements of the Unloaded Unfolding Rate. Previous work has determined the unfolding rate of DNA and RNA hairpins at zero load for a variety of short DNA and RNA hairpins, as well as a couple of longer RNA hairpins, using both micromechanical and fluorescence-based approaches. In Fig. 7, we compare these results with our own values for the unloaded unfolding rates ($k_{u,0}$) of tetraloop DNA hairpins with 50% stem GC content. Precise comparisons are problematic because of the different sequences, temperatures, and buffer conditions used; nevertheless, the current data set agrees well with the previous results for both short and long hairpins, connecting these otherwise disparate measurements and extending them over several orders of magnitude.

A previous study (not shown in Fig. 7) also measured the thermal dissociation of AU helices 8-18 bp long (9). Extrapolation of those results to a 20-bp helix results in a dissociation rate of $\sim 10^{-3 \pm 1}$ s^{-1} ($\ln k \approx -7 \pm 2$), in reasonable agreement with the value $\ln k_{u,0} = -10 \pm 1$ derived from our measurement of a hairpin with the same stem length and GC content (20R0/T4).

1. Tinoco, I., Jr. & Bustamante, C. (2002) *Biophys. Chem.* **101-102**, 513-533.
2. Liphardt, J., Onoa, B., Smith, S. B., Tinoco, I., Jr., & Bustamante, C. (2001) *Science* **292**, 733-737.
3. Dessinges, M.-N., Maier, B., Zhang, Y., Peliti, M., Bensimon, D. & Croquette, V. (2002) *Phys. Rev. Lett.* **84**, 248102.
4. Marko, J. F. & Siggia, E. D. (1995) *Macromolecules* **28**, 8759-8770.
5. Campa, A. & Giansanti, A. (1998) *Phys. Rev. E* **58**, 3585-3588.
6. van Dongen, M. J., Mooren, M. M., Willems, E. F., van der Marel, G. D., van Boom, J. H. Wijmenga, S. S. & Hilbers, C. W. (1997) *Nucleic Acids Res*. **25**, 1537-1547.
7. Nakano, M, Moody, E. M., Liang, J., & Bevilacqua, P. C. (2002) *Biochemistry* **41**, 14281-14292.
8. Abbondanzieri, E. A., Shaevitz. J. W. & Block, S. M. (2005) *Biophys. J*. **89**: L61-L63.
9. Pörschke, D. (1977*) Mol. Biol. Biochem. Biophys*. **24**, 191-218.

Table 2 Hairpins studied

Name	Hairpin sequence	*n*
6R50/4T	GAGCTA(T)$_4$TAGCTC	6 (8)
8R50/4T	GAGTCCTA(T)$_4$TAGGACTC	5
10R50/4T	GAGTCTCCTA(T)$_4$TAGGAGACTC	7
15R50/4T	GAGTCCTGGATCCTA(T)$_4$TAGGATCCAGGACTC	9 (10)
20R50/4T	GAGTCAACGTCTGGATCCTA(T)$_4$TAGGATCCAGACGTTGACTC	7 (11)
25R50/4T	GAGTCAACGTTCACGCTGGATCCTA(T)$_4$TAGGATCCAGCGTGAACGTTGACTC	9 (10)
30R50/4T	GAGTCAACGTACTGATCACGCTGGATCCTA(T)$_4$TAGGATCCAGCGTGATCAGTACGTTGACTC	10
15R60/3T	GAGTCCTGGATCCTG(T)$_3$CAGGATCCAGGACTC	3
15R60/4T	GAGTCCTGGATCCTG(T)$_4$CAGGATCCAGGACTC	7
15R60/6T	GAGTCCTGGATCCTG(T)$_6$CAGGATCCAGGACTC	6 (7)
15R60/8T	GAGTCCTGGATCCTG(T)$_8$CAGGATCCAGGACTC	8
15R60/12T	GAGTCCTGGATCCTG(T)$_{12}$CAGGATCCAGGACTC	6 (11)
15R60/15T	GAGTCCTGGATCCTG(T)$_{15}$CAGGATCCAGGACTC	6 (8)
15R60/20T	GAGTCCTGGATCCTG(T)$_{20}$CAGGATCCAGGACTC	1 (5)
15R60/30T	GAGTCCTGGATCCTG(T)$_{30}$CAGGATCCAGGACTC	0 (4)
20R0/4T	TATTATATATTAATATATAA(T)$_4$TTATATATTAATATATAATA	10
20R25/4T	AAGTTAACATCTAGATTCTA(T)$_4$TAGAATCTAGATGTTAACTT	2 (3)
20R55/4T	GAGTCAACGTCTGGATCCTG(T)$_4$CAGGATCCAGACGTTGACTC	10
20R75/4T	GGTGCACCGTCCGGACCCTG(T)$_4$CAGGGTCCGGACGGTGCACC	6
20R100/4T	CGCCGCGGGCCGGCGCGCGG(T)$_4$CCGCGCGCCGGCCCGCGGCG	8 (9)

Table 1 Numerical results from experiment and model

First set of values for each hairpin indicates the experimental results. Model results are shown below in italics.

Hairpin name	Δx, nm	$F_{1/2}$, pN	ΔG, kJ/mol	$\ln(k_{u,0})$,s^{-1}	$\ln(\tau_{1/2})$, s	$\Delta x^{\ddagger}_{f}$, nm	$\Delta x^{\ddagger}_{u}$, nm
6R50/T4	5.1 ± 0.3 *5.8 ± 0.2*	8.0 ± 0.7 *7.8 ± 0.4*	25 ± 3 *29 ± 2*	2.4 ± 0.5 *4.3 ± 0.6*	-6.0 ± 0.1 *-5.8 ± 0.2*	2.2 ± 0.2 *2.6 ± 0.6*	2.8 ± 0.2 *3.2 ± 0.6*
8R50/T4	7.2 ± 0.3 *7.6 ± 0.3*	8.4 ± 0.6 *9.2 ± 0.4*	38 ± 3 *43 ± 3*	0.4 ± 0.3 *0.6 ± 0.9*	-5.4 ± 0.1 *-5.0 ± 0.3*	3.4 ± 0.3 *4.0 ± 0.8*	3.8 ± 0.4 *3.5 ± 0.8*
10R50/T4	8.7 ± 0.3 *9.4 ± 0.4*	10.5 ± 0.6 *10.2 ± 0.5*	54 ± 4 *58 ± 4*	-4.1 ± 0.6 *-3.7 ± 1.1*	-4.7 ± 0.1 *-4.3 ± 0.3*	5.1 ± 0.4 *5.7 ± 0.8*	4.0 ± 0.4 *3.8 ± 0.8*
15R53/T4	13.6 ± 0.3 *13.9 ± 0.5*	12.3 ± 0.4 *12.0 ± 0.5*	100 ± 6 *100 ± 6*	-12 ± 2 *-16 ± 2*	-3.4 ± 0.2 *-3.0 ± 0.3*	7.9 ± 0.5 *9.5 ± 1.1*	5.4 ± 0.4 *4.4 ± 1.1*
20R50/T4	17.8 ± 0.3 *18.2 ± 0.6*	13.6 ± 0.4 *12.9 ± 0.5*	146 ± 8 *140 ± 9*	-29 ± 2 *-27 ± 3*	-2.2 ± 0.2 *-2.4 ± 0.4*	12.5 ± 0.7 *13.2 ± 1.2*	5.6 ± 0.5 *5.0 ± 1.2*
25R52/T4	20.9 ± 0.5 *22.4 ± 0.8*	14.5 ± 0.7 *13.9 ± 0.6*	183 ± 10 *183 ± 11*	-37 ± 3 *-39 ± 3*	-1.3 ± 0.2 *-1.4 ± 0.4*	14.6 ± 0.9 *17.0 ± 1.2*	6.3 ± 0.5 *5.5 ± 1.2*
30R50/T4	26.5 ± 0.5 *27.0 ± 1.0*	14.4 ± 0.7 *13.9 ± 0.6*	227 ± 11 *218 ± 14*	-53 ± 5 *-49 ± 4*	-1.2 ± 0.2 *-1.5 ± 0.4*	19.7 ± 1.2 *21.2 ± 1.2*	6.7 ± 0.5 *5.9 ± 1.2*
15R60/T3	13.0 ± 0.5 *13.2 ± 0.4*	10.8 ± 0.8 *12.3 ± 0.5*	91 ± 9 *95 ± 6*	-15 ± 2 *-17 ± 2*	-4.0 ± 0.3 *-3.6 ± 0.3*	7.9 ± 0.5 *9.2 ± 1.1*	5.4 ± 0.7 *4.3 ± 1.1*
15R60/T4	13.5 ± 0.3 *13.6 ± 0.5*	13.3 ± 0.5 *12.8 ± 0.5*	108 ± 6 *102 ± 6*	-19 ± 2 *-16 ± 2*	-3.9 ± 0.2 *-4.7 ± 0.3*	8.5 ± 0.4 *9.5 ± 1.1*	4.8 ± 0.3 *4.3 ± 1.1*
15R60/T6	14.8 ± 0.3 *14.5 ± 0.5*	11.3 ± 0.7 *11.7 ± 0.5*	100 ± 6 *100 ± 6*	-17 ± 3 *-18 ± 2*	-2.2 ± 0.4 *-2.3 ± 0.4*	8.7 ± 0.6 *9.4 ± 1.1*	6.2 ± 0.7 *5.2 ± 1.1*
15R60/T8	15.2 ± 0.5 *15.3 ± 0.5*	10.3 ± 0.5 *11.1 ± 0.4*	95 ± 7 *101 ± 6*	-13 ± 2 *-18 ± 2*	-1.4 ± 0.3 *-0.8 ± 0.4*	7.9 ± 0.7 *9.5 ± 1.1*	8.0 ± 0.7 *5.8 ± 1.1*
15R60/T12	17.3 ± 0.5 *16.8 ± 0.5*	9.7 ± 0.5 *10.1 ± 0.4*	98 ± 7 *103 ± 6*	-15 ± 3 *-19 ± 2*	1.9 ± 0.4 *1.2 ± 0.5*	8.6 ± 0.7 *9.4 ± 1.1*	8.1 ± 0.6 *7.3 ± 1.1*
15R60/T15	18.6 ± 0.6 *17.9 ± 0.6*	9.1 ± 0.8 *9.5 ± 0.4*	98 ± 10 *104 ± 7*	-14 ± 3 *-19 ± 2*	3.0 ± 0.4 *2.6 ± 0.6*	9.8 ± 1.1 *9.5 ± 1.1*	9.1 ± 1 *8.2 ± 1.1*

15R60/T20	20.8 ± 0.7 *19.7 ± 0.7*	8.1 ± 0.9 *8.7 ± 0.4*	90 ± 12 *104 ± 7*	-9 ± 6 *-19 ± 2*	5.0 ± 0.3 *4.3 ± 0.6*	8.9 ± 1.3 *9.3 ± 1.1*	11.6 ± 1.6 *9.9 ± 1.1*
15R60/T30	25.7 ± 1 *23.5 ± 0.8*	7 ± 1 *7.3 ± 0.3*	96 ± 25 *104 ± 7*	NA *-20 ± 2*	>7 ± 0.7 *7.0 ± 0.7*	NA *9.1 ± 1.1*	NA *12.9 ± 1.1*
20R0/T4	17.6 ± 0.3 *16.5 ± 0.5*	7.9 ± 0.4 *8.8 ± 0.4*	86 ± 5 *83 ± 5*	-10 ± 1 *-9.3 ± 1.5*	-4.2 ± 0.4 *-6.0 ± 0.2*	10.9 ± 0.7 *11.6 ± 1.1*	6.0 ± 0.5 *5.3 ± 1.1*
20R25/T4	17.6 ± 0.4 *17.5 ± 0.6*	10.6 ± 0.5 *11.1 ± 0.5*	112 ± 8 *112 ± 7*	-23 ± 3 *-20 ± 2*	-2.6 ± 0.5 *-4.2 ± 0.3*	11.7 ± 0.8 *12.9 ± 1.2*	5.6 ± 0.8 *5.0 ± 1.2*
20R55/T4	18.1 ± 0.3 *17.9 ± 0.7*	13.8 ± 0.4 *13.5 ± 0.6*	146 ± 7 *140 ± 9*	-31 ± 2 *-27 ± 3*	-2.9 ± 0.3 *-4.2 ± 0.3*	12.5 ± 0.7 *13.0 ± 1.2*	5.6 ± 0.7 *4.9 ± 1.2*
20R75/T4	19.3 ± 0.4 *18.6 ± 0.7*	15.2 ± 0.5 *15.1 ± 0.6*	175 ± 10 *165 ± 10*	-36 ± 2 *-36 ± 3*	-2.5 ± 0.3 *-2.2 ± 0.4*	12.3 ± 0.7 *13.7 ± 1.2*	6.1 ± 0.7 *5.1 ± 1.2*
20R100/T4	19.0 ± 0.4 *19.5 ± 0.8*	19.3 ± 0.8 *18.0 ± 0.7*	220 ± 13 *207 ± 13*	-43 ± 3 *-51 ± 4*	-2.6 ± 0.3 *-0.5 ± 0.4*	13.3 ± 0.7 *14.7 ± 1.2*	5.8 ± 0.4 *4.9 ± 1.2*

Supporting Information Figure Captions

Fig. 4. Lifetimes of unfolded state for hairpin 20R55/T4 under constant load, shown at two different forces. Lifetimes are exponentially distributed and depend on the force applied.

Fig. 5. Effect of externally-applied force on the free-energy landscape of a two-state system. Force tilts the landscape by an amount $\Delta G = F_0 \Delta x$, changing the free energy of both the transition state and the unfolded state, and thereby the folding and unfolding rates, as well as the relative populations of folded and unfolded states. Variable labels are defined in the text.

Fig. 6. Representative records of hairpin extension vs. time and extension histograms for hairpins under constant load, adjusted in each case to be near the associated unzipping force, $F_{1/2}$. (*A*) Comparison of hairpins with varying stem length. The most rapidly fluctuating of these, hairpin 8R50/T4, was measured in an open-loop configuration (see *Methods*). (*B*) Comparison of hairpins with varying loop length. (*C*) Comparison of hairpins with varying stem GC content.

Fig. 7. Comparison of unfolding rates at zero force with previous work. Measurements of $k_{u,0}$ for tetraloop hairpins with varying stem length and 50% GC content are compared with previous results for the unloaded or thermal unfolding rate of DNA and RNA hairpins. Filled shapes denote DNA hairpin data and open shapes denote RNA data; squares denote force-induced unfolding measurements and circles represent thermal unfolding measurements. References are color-coded as indicated. Sequences and temperatures vary. Ref. 1, sequences r(GC-UUCG-GC) and r(GC-UUCG-GC), 37.5ºC; r(GGAC-UUCG-GUCC) and r(GGAC-UUUU-GUCC), 65ºC. Ref. 2, r(GGGC-G(2AP)AA-GCCUUAU), 8ºC. Ref. 3, AACCC-T_{21}-GGGTT, 25ºC. Ref. 4, ATCCTA-T_4-TAGGAT, 54ºC. Ref. 5, GGATAA-T_4-TTATCC, extrapolated from data to 23ºC. Ref. 6, r(AAAAAA-C_6-UUUUUU), interpolated from data to 23ºC. Ref. 7, CGGATAA-T_8-TTATCCG, 36ºC. Ref. 8, CCCAA-T_n-TTGGG, extrapolated from data to n=4 (tetraloop), 23ºC.

Ref. 9, GGGTT-A_{30}-AACCC, 23ºC. Ref. 10, CTCTTCA-A_{40}-TGAAGAG and CTCTTCAGT-A_{40}-ACTGAAGAG, room temperature. Ref. 11, HIV TAR hairpin r(GGCUCGGUUAGACCAGAUCUGAGC-CUGGGA-GCUCUCUGGCUAACUAGGGCC), room temperature. Ref. 12, P5ab hairpin from *T. thermophila* ribozyme, r(CCGUUCAGUACCAAGUCUCAGGG-GAAA-CUUUGAGAUGGGGUGCUGACGG), room temperature.

1. Proctor, D. J., Ma, H., Kierzek, E., Kierzek, R., Gruebele, M. & Bevilacqua, P. C. (2004) *Biochemistry* **43**, 14004-14014.
2. Menger, M., Eckstein, F.& Pörschke, D. (2000) *Biochemistry* **39**, 4500-4507.
3. Jung, J. & van Orden, A. (2005) *J. Phys. Chem B* **109**, 3648-3657.
4. Hilbers, C. W., Haasnoot, C. A., de Bruin, S. H., Joordens, J. J., van der Marel G. A. & van Boom, J. H. (1985) *Biochimie* **67**, 685-695.
5. Ansari, A., Kuznetsov, S., & Shen, Y. (2001) *Proc. Natl. Acad. Sci. USA* **98**, 7771-7776.
6. Pörschke, D. (1977*) Mol. Biol. Biochem. Biophys*. **24**, 191-218.
7. Ansari, A., & Kuznetsov, S. (2005) *J. Phys. Chem. B* **109**, 12982-12989.
8. Bonnet, G., Krichevsky, O., & Libchaber, A. (1998) *Proc. Natl. Acad. Sci. USA* **95**, 8602-8606 (1998).
9. Wallace, M. I., Ying, L., Balasubramanian, S., & Klenerman, D. (2001) *Proc. Natl. Acad. Sci. USA* **98**, 5584-5589.
10. Grunwell, J. R., Glass, J. L., Lacoste, T. D., Deniz, A. A., Chemla, D. S., & Schultz, P. G. (2001) *J. Am. Chem. Soc.* **123**, 4295-4303 (2001).
11. Li, P. T. X., Collin, D., Smith, S. B., Bustamante, C. & Tinoco, I., Jr. (2006) *Biophys. J*. **90**, 250-260.
12. Liphardt, J., Onoa, B., Smith, S. B., Tinoco, I., Jr., & Bustamante, C. (2001) *Science* **292**, 733-737.

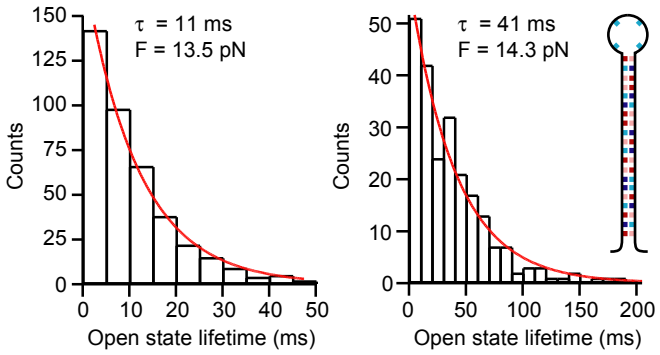
τ = 11 ms
F = 13.5 pN
Counts
Open state lifetime (ms)
τ = 41 ms
F = 14.3 pN
Counts
Open state lifetime (ms)

Fig. 4

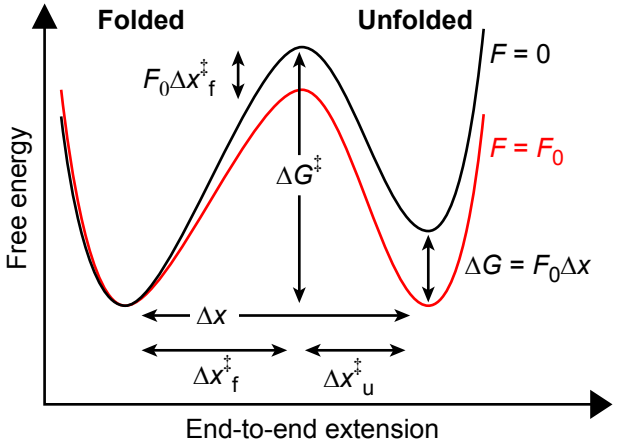
Folded
Unfolded
F = 0
F = F0
ΔG‡
ΔG = F0Δx
Δx
Free energy
End-to-end extension

Fig. 5

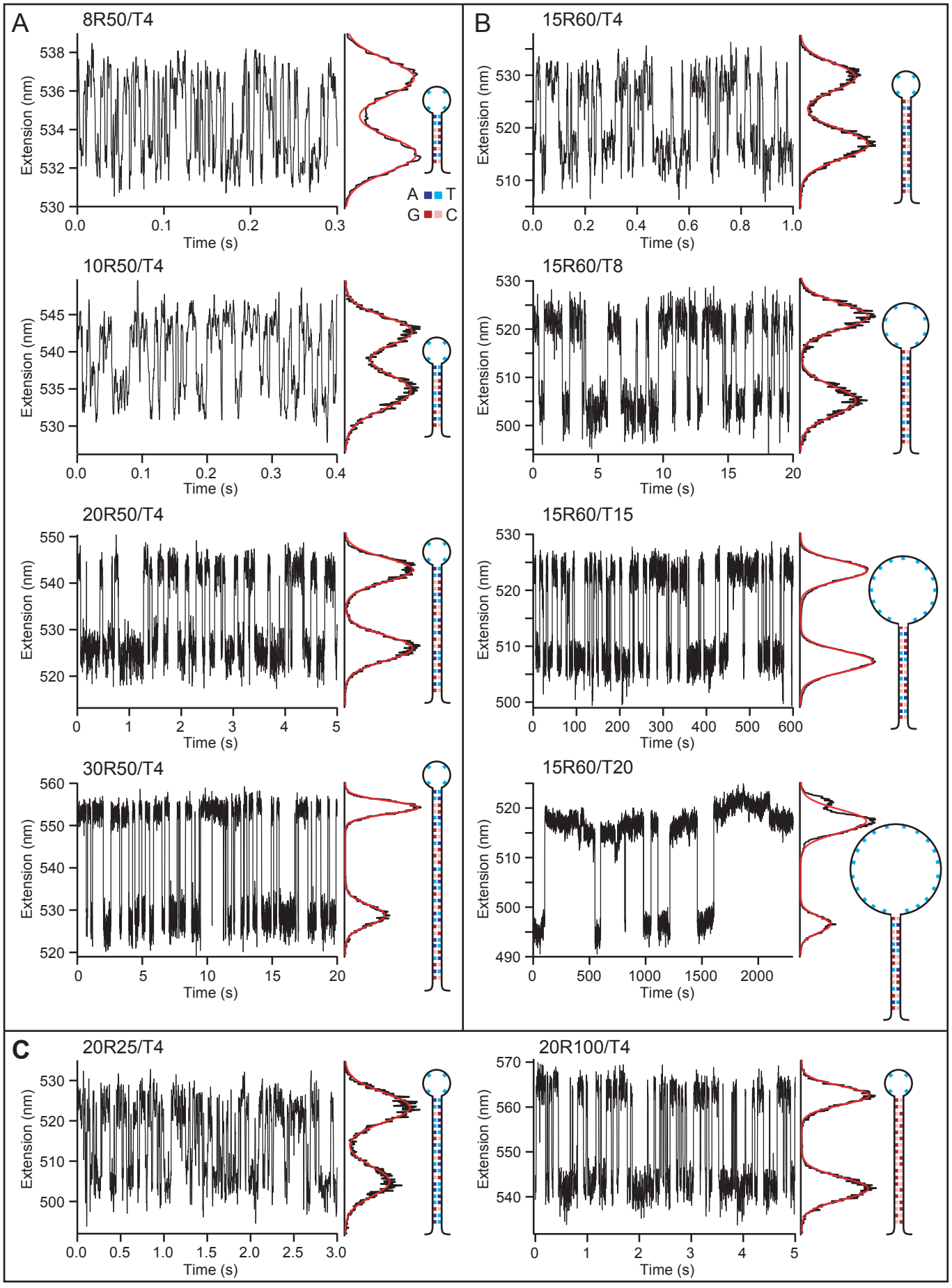
A
8R50/T4
Extension (nm)
Time (s)
A T
G C
10R50/T4
20R50/T4
30R50/T4
B
15R60/T4
15R60/T8
15R60/T15
15R60/T20
C
20R25/T4
20R100/T4

Fig. 6

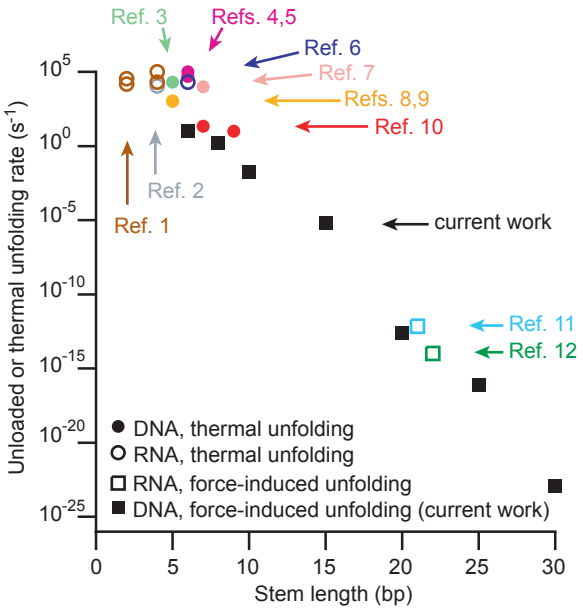
Ref. 3
Refs. 4,5
Ref. 6
Ref. 7
Refs. 8,9
Ref. 10
Ref. 2
Ref. 1
current work
Ref. 11
Ref. 12
DNA, thermal unfolding
RNA, thermal unfolding
RNA, force-induced unfolding
DNA, force-induced unfolding (current work)
Unloaded or thermal unfolding rate (s-1)
Stem length (bp)
10^5
10^0
10^-5
10^-10
10^-15
10^-20
10^-25
0
5
10
15
20
25
30

Fig. 7